Cu-ATC vs. Cu-BTC: Comparing the H_2 Adsorption Mechanism Through Experiment, Molecular Simulation, and Inelastic Neutron Scattering Studies

Tony Pham,[*,†,§] Katherine A. Forrest,[†,§] Zheng Niu,[‡] Brant Tudor,[†] Chloe B. Starkey,[†] Yue Wang,[‡] Mohamed Eddaoudi,[○] Nathaniel Rosi,[⊥] Gisela Orcajo,[∥] Juergen Eckert,[*,†,▽] Shengqian Ma,[◇] and Brian Space[*,†,□]

[†]*Department of Chemistry, University of South Florida, 4202 East Fowler Avenue, CHE205, Tampa, Florida 33620-5250, United States*

[‡]*College of Chemistry, Chemical Engineering and Materials Science, Soochow University, Suzhou, Jiangsu 215123, Republic of China*

[○]*Advanced Membranes and Porous Materials Center, Division of Physical Sciences and Engineering, 4700 King Abdullah University of Science and Technology, Thuwal 23955-6900, Kingdom of Saudi Arabia*

[⊥]*Department of Chemistry, University of Pittsburgh, Chevron Science Center, 219 Parkman Avenue, Pittsburgh, Pennsylvania 15260, United States*

[∥]*Department of Chemical and Energy Technology, ESCET, Rey Juan Carlos University, C/Tulipán s/n, 28933 Móstoles, Madrid, Spain*

[▽]*Department of Chemistry and Biochemistry, Texas Tech University, 2500 Broadway, Box 41061, Lubbock, Texas 79409-1061, United States*

[◇]*Department of Chemistry, University of North Texas, 1508 West Mulberry Street, Denton, Texas 76201, United States*

[□]*Department of Chemistry, North Carolina State University, 2700 Stinson Drive, Cox Hall 506, Raleigh, North Carolina 27607, United States*

[§]Authors contributed equally

[*]tpham4@mail.usf.edu; juergen@usf.edu; bspace@ncsu.edu

Cu-ATC Fragments

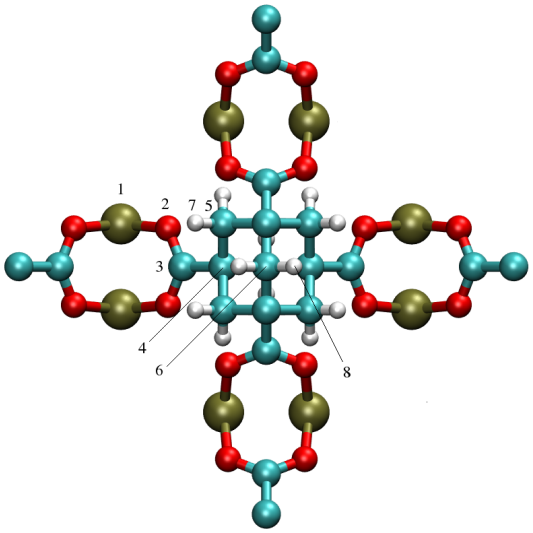

Figure S1. The numbering of the chemically distinct atoms in Cu-ATC as referred to in Table S1. Atom colors: C = cyan, H = white, O = red, Cu = tan.

Figure S2. Fragments of Cu-ATC that were selected for gas phase charge fitting calculations. Numerical labeling corresponds to chemically distinct atoms evaluated. Atom colors: C = cyan, H = white, O = red, Cu = tan.

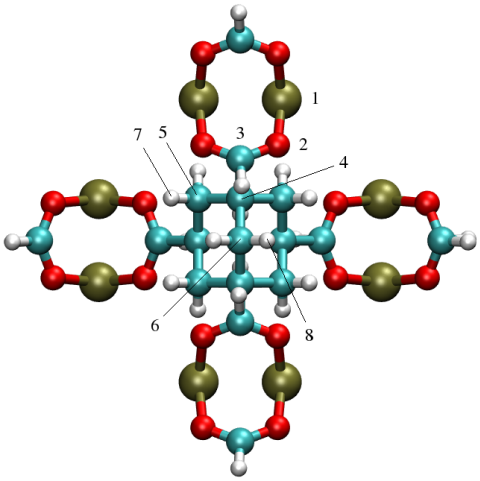

(a) Fragment 1

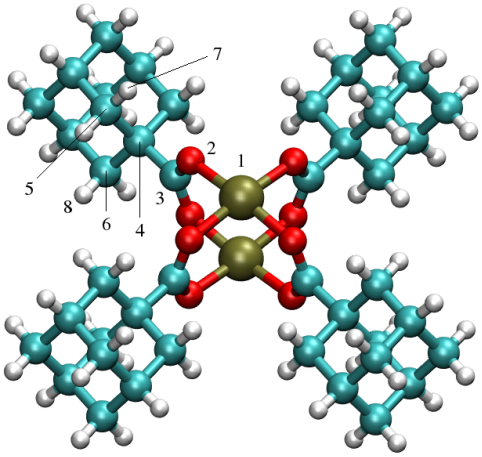

(b) Fragment 2

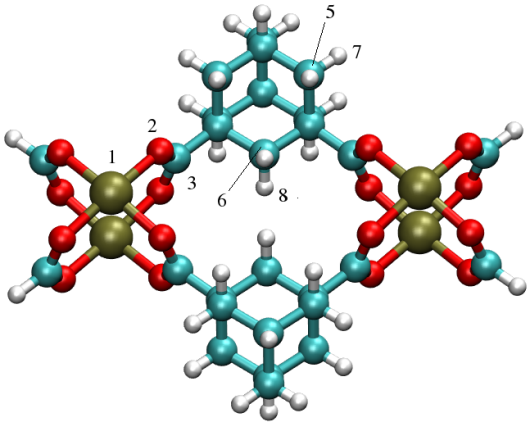

(c) Fragment 3

Table S1. Comparison of partial charges (e^-) for the series of gas phase fragments that were selected for Cu-ATC as shown in Figure S2. Labeling of atoms corresponds to Figure S1.

Atom	Label	Frag 1	Frag 2	Frag 3
Cu	1	1.2109	1.1033	1.1948
O	2	-0.7753	-0.7678	-0.7850
C	3	0.8932	0.8440	0.8611
C	4	0.1350	0.2943	0.2502
C	5	-0.1370	-0.2207	-0.1500
C	6	-0.0082	-0.1017	-0.1365
H	7	0.0460	0.0285	0.0286
H	8	-0.0022	0.0059	0.0268

Cu-BTC Fragments

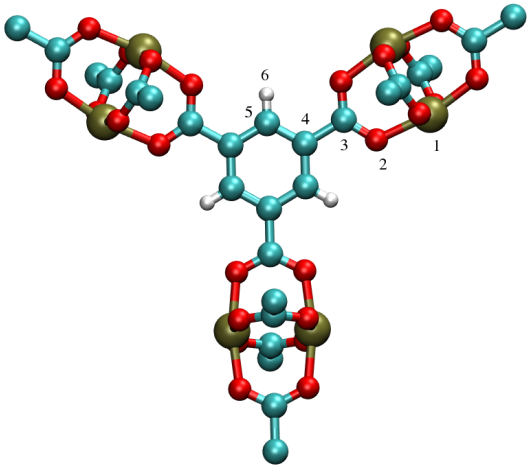

Figure S3. The numbering of the chemically distinct atoms in Cu-ATC as referred to in Table S2. Atom colors: C = cyan, H = white, O = red, Cu = tan.

Table S2. Comparison of partial charges (e^-) for the series of gas phase fragments that were selected for Cu-BTC as shown in Figure S4. Labeling of atoms corresponds to Figure S3.

Atom	Label	Frag 1	Frag 2	Frag 3	Frag 4	Frag 5	Frag 6	Frag 7	Frag 8
Cu	1	1.2168	1.0606	1.0189	1.0803	1.0798	0.9767	1.0423	1.1456
O	2	-0.7710	-0.7598	-0.6948	-0.7048	-0.6998	-0.6970	-0.7625	-0.7494
C	3	0.9672	0.9803	0.8860	0.9132	0.9064	0.8941	0.9420	0.9669
C	4	-0.1927	-0.2294	-0.1949	-0.2350	-0.2161	-	-	-0.2066
C	5	-0.0115	0.0178	0.0049	0.0487	0.0248	-	-	-0.0278
H	6	0.1886	0.1821	0.1770	0.1622	0.1691	-	-	0.1893

Figure S4. Fragments of Cu-BTC that were selected for gas phase charge fitting calculations. Numerical labeling corresponds to chemically distinct atoms evaluated. Atom colors: C = cyan, H = white, O = red, Cu = tan.

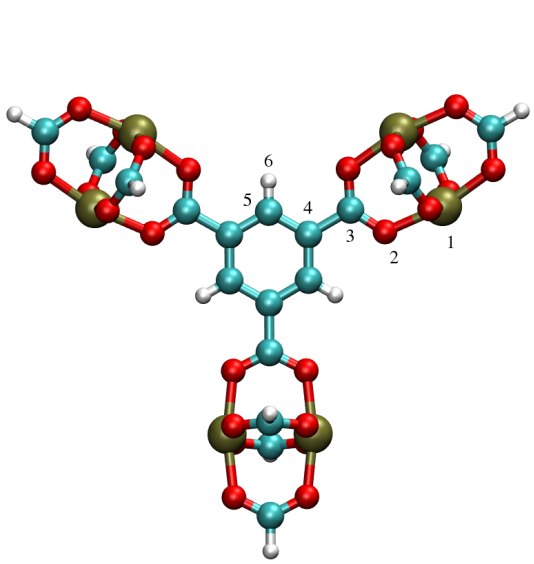

(a) Fragment 1

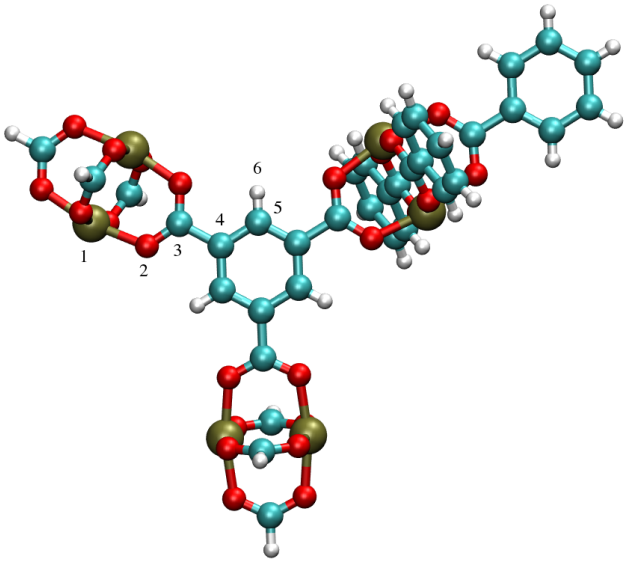

(b) Fragment 2

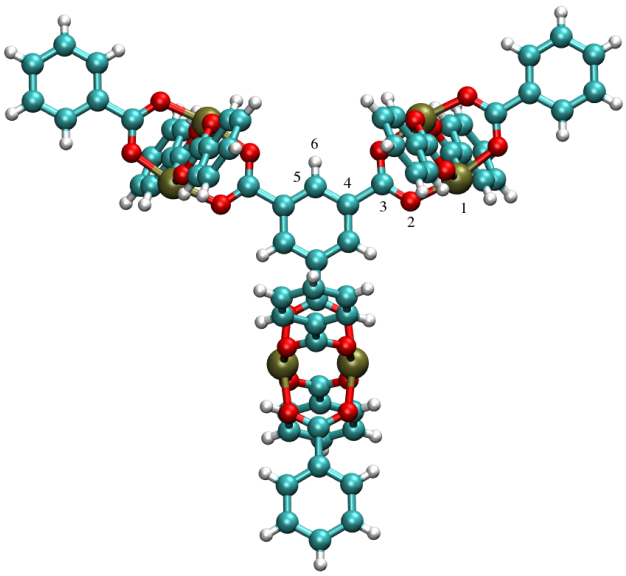

(c) Fragment 3

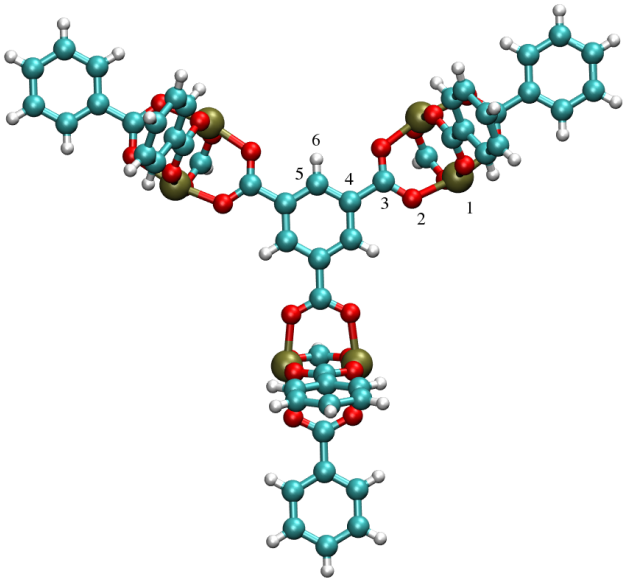

(d) Fragment 4

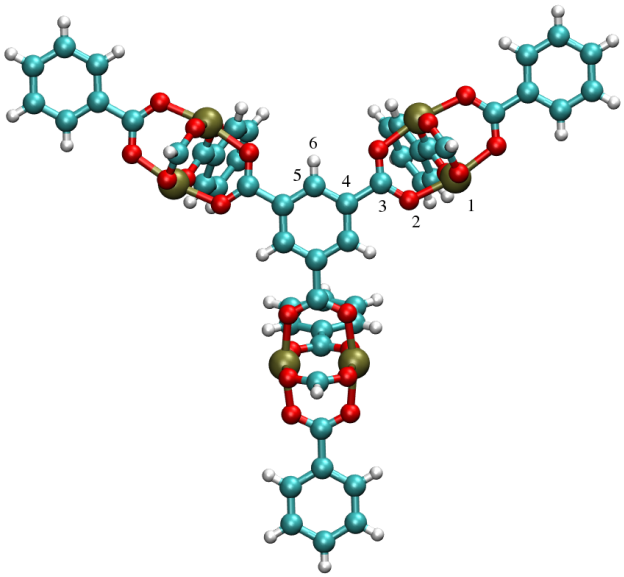

(e) Fragment 5

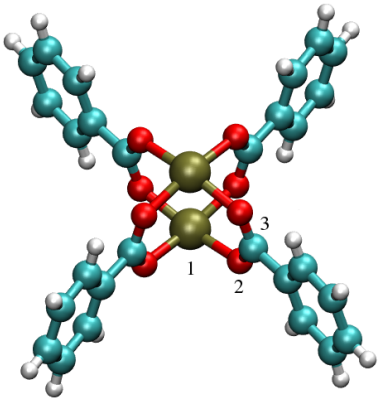

(f) Fragment 6

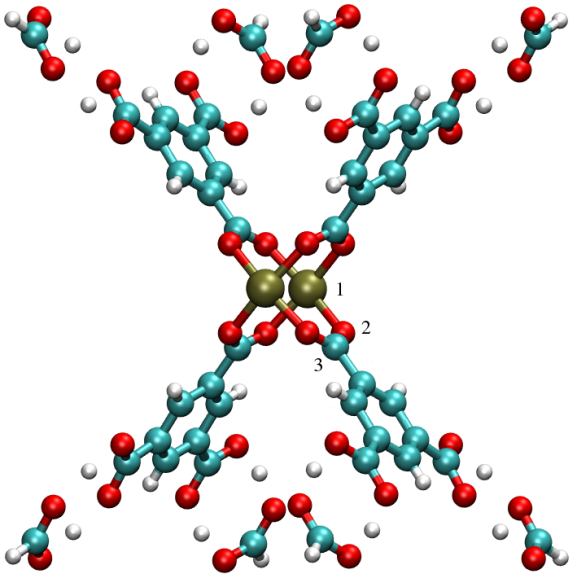

(g) Fragment 7

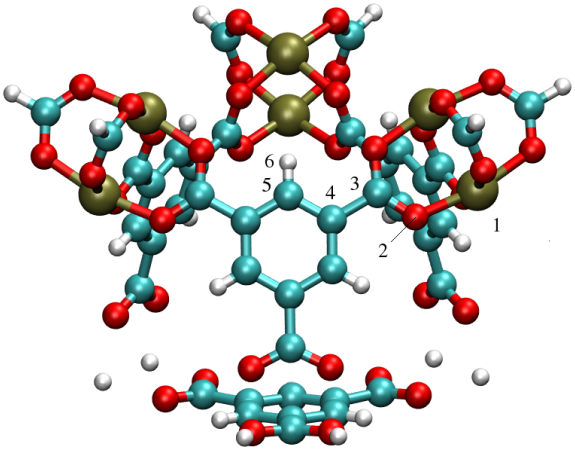

(h) Fragment 8

Experimental Synthesis and Characterization

1,3,5,7-adamantanetetracarboxylic acid (H_4ATC) was synthesized according to previously reported methods.[1,2] The hydrated form of Cu-ATC (Cu_2(ATC)($2H_2O$)·$5H_2O$) was synthesized according to the procedure reported in reference 3 with slight modification.[4–6] A mixture of H_4ATC (0.035 g, 0.11 mmol) and $Cu(NO_3)_2$·$2.5H_2O$ (0.077 g, 0.33 mmol) dissolved in 3 mL of an aqueous 0.001 M NaOH solution was heated to 100 °C to obtain a clear blue solution. The aqueous solution was then heated to 200 °C for 18 h to produce green crystals of hydrated Cu-ATC along with small amounts of crystalline H_4ATC. The solid was filtered and subsequently washed with hot water several times to obtain purified crystals in 46% yield.

Crystals of Cu_2(ATC)($2H_2O$)·$5H_2O$ were soaked in anhydrous CH_3OH for 2 days with fresh CH_3OH five times.[4] The crystals were then vacuumed at room temperature until the pressure decreased to 3 μmHg. At this point, the temperature was increased to 120 °C and the crystals were vacuumed for 5 h. After the pressure decreased to below 3 μmHg, the temperature was increased to 190 °C and the crystals were vacuumed for 12 h to yield dark purple crystals of anhydrous Cu-ATC.

Powder X-ray diffraction (PXRD) analysis on the as-synthesized and activated samples of Cu-ATC were carried out at room temperature on a PANalytical Aeris diffractometer with Cu-Kα radiation (λ = 1.5406 Å). 2θ scans were performed between 3° and 50° with a step size of 0.02°. The resulting patterns of the as-synthesized and activated samples are shown in Figures S5(a) and S5(b), respectively.The experimental PXRD patterns are in good agreement with the corresponding patterns that have been calculated from single crystal data.[3]

Thermal gravimetric analysis (TGA) of as-synthesized Cu-ATC was performed on a Mettler TGA/SDTA851 thermal analyzer under an N_2 atmosphere with a heating rate of 5 °C min^{-1}. Figure S6 shows the resulting TGA curve of the sample from room temperature to 800 °C.

All low-pressure gas adsorption measurements on activated samples of Cu-ATC were performed using a Micromeritics ASAP 2020 Surface Area and Porosity Analyzer equipped with a turbo molecular vacuum pump. A pore size distribution plot for Cu-ATC was obtained based on N_2 adsorption measurements at 77 K (Figure S7).

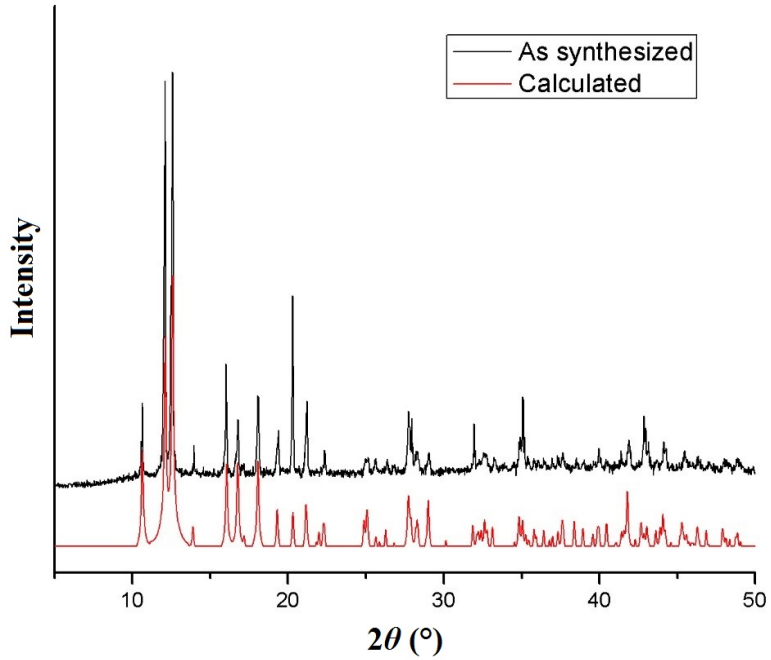

(a) As-synthesized

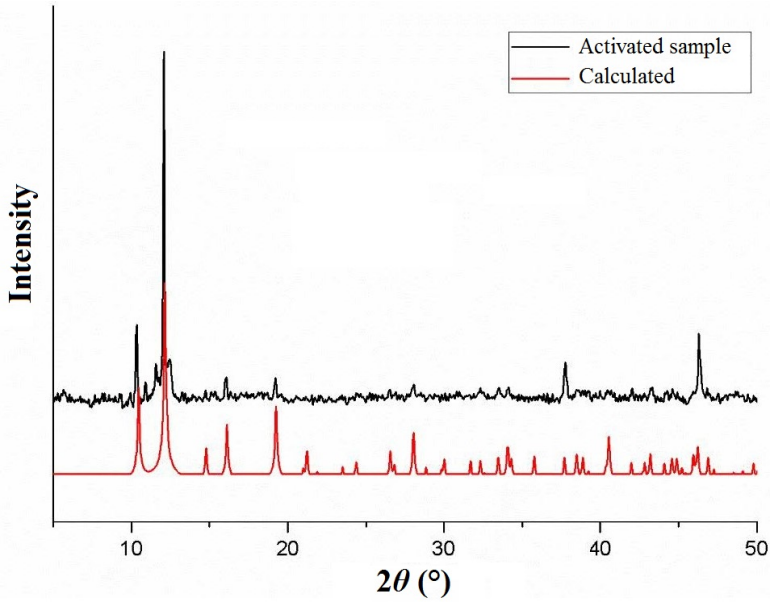

(b) Activated

Figure S5. Experimental (black) and calculated (red) powder X-ray diffraction (PXRD) patterns of **(a)** $Cu_2(ATC)(2H_2O)\cdot 5H_2O$ and **(b)** activated Cu-ATC. The simulated PXRD patterns were obtained based on calculations on the hydrated and dehydrated crystal structures of Cu-ATC as reported in reference 3.

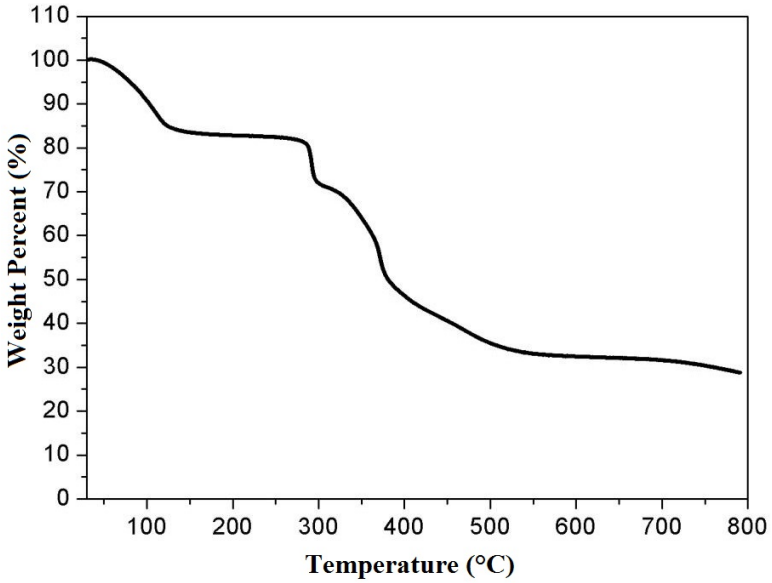

Figure S6. Thermal gravimetric analysis (TGA) curve of $Cu_2(ATC)(2H_2O)\cdot 5H_2O$ from room temperature to 800 °C.

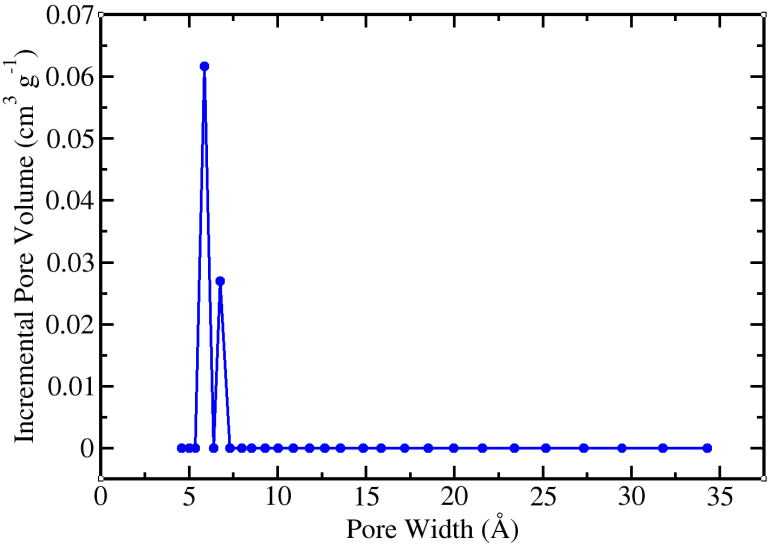

Figure S7. The pore size distribution of Cu-ATC.

Experimental Isosteric Heat of Adsorption for H_2 in Cu-ATC

The experimental Q_{st} values for H_2 in Cu-ATC were determined for a range of loadings by applying the virial method[7,8] to the experimental adsorption isotherms at 77 and 87 K. The isotherm data were simultaneously fitted to the following equation:

$$\ln P = \ln N + \left(\frac{1}{T}\right)\sum_{i=0}^{m} a_i N^i + \sum_{j=0}^{n} b_j N^j \tag{1}$$

where P is the pressure (in torr), N is the amount adsorbed (in mmol g^{-1}), T is the temperature (in K), a_i and b_i are the temperature-independent virial coefficients, and m and n represent the number of coefficients required to fit the isotherm data. The equation was fit using the R statistical software package.[9] The values of the virial coefficients a_0 through a_m were then used to calculate the Q_{st} using the following equation:

$$Q_{st} = -R\sum_{i=0}^{m} a_i N^i \tag{2}$$

where R is the ideal gas constant. The parameters that were obtained through virial fitting of the experimental isotherms for H_2 in Cu-ATC are provided in Table S3. Figure S8 shows the overall fit to the H_2 adsorption isotherms by the virial equation.

Table S3. Parameters that were obtained through virial fitting of the experimental H_2 adsorption isotherms for Cu-ATC. The R^2 value is also provided.

Parameter	Value
a_0	-1520.7575568249
a_1	136.252706043799
a_2	10.7887388579273
a_3	-10.6657394125275
a_4	1.30990077590925
a_5	-0.0485437241608287
b_0	17.2813218787081
b_1	-0.960936658756897
b_2	0.223835811080939
R^2	0.999627104

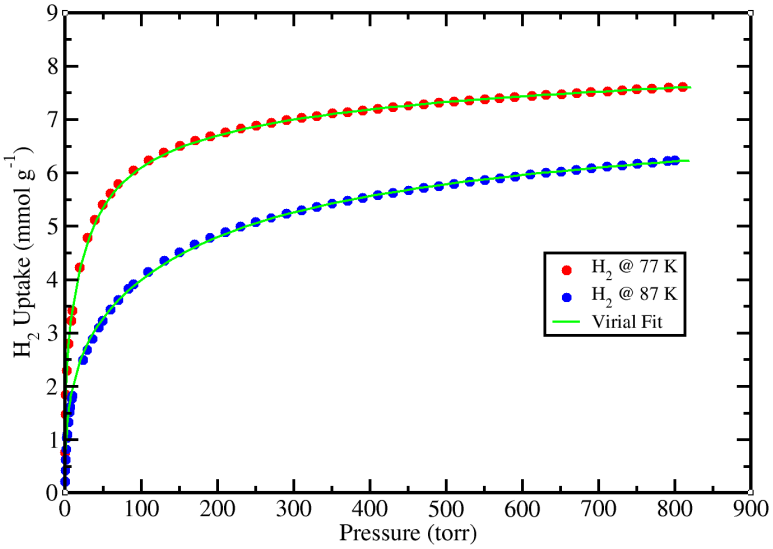

Figure S8. Experimental H_2 adsorption isotherms at 77 K (red circles) and 87 K (blue circles) and the virial equation fits (solid green lines) for Cu-ATC.

Cycling Performance Experiment

Crystalline samples (80–100 mg) of anhydrous Cu-ATC were activated according to previously reported methods[3,4] and transferred to a pre-weighed 6-mm large glass bulb sample cell. The sample was degassed at 190 °C under high vacuum (< 5 μmHg) for 16 h prior to H_2 adsorption analysis. During this time, a color change from blue to dark purple occurred for the sample. The low-pressure H_2 adsorption isotherms were collected on a Micromeritics ASAP 2020 surface area and porosity analyzer equipped with a turbo molecular vacuum pump at 77 K after activation of Cu-ATC. After the initial low-pressure H_2 adsorption measurement, the sample was directly subjected to another adsorption cycle at 77 K without the degassing process. Figure S9 shows the result of this cycling experiment for H_2 in Cu-ATC at 77 K.

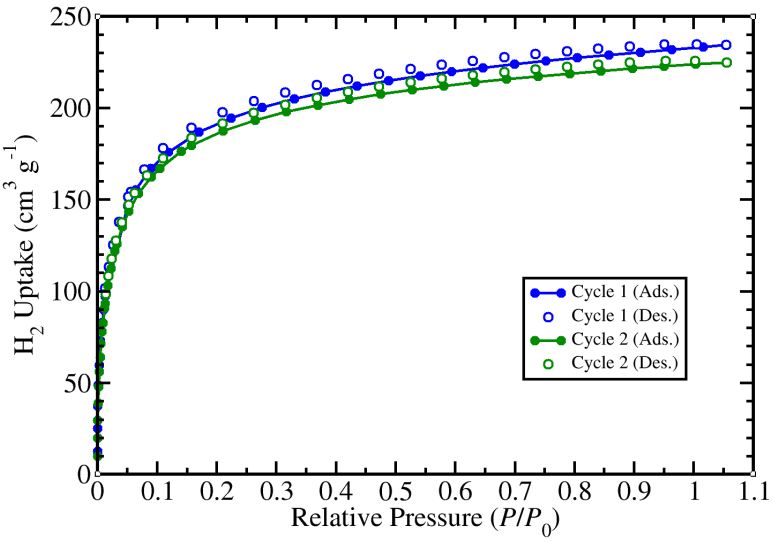

Figure S9. Experimental H_2 adsorption (closed circles with lines) and desorption (open circles) isotherms for the first (blue) and second (green) adsorption cycles in Cu-ATC at 77 K.

Periodic Density Functional Theory

Periodic density functional theory (DFT) calculations were performed to optimize (1) a single unit cell of Cu-ATC with H_2 localized between two Cu^{2+} ions of adjacent copper paddlewheels and (2) a unit cell of Cu-BTC with H_2 positioned about a lone Cu^{2+} ion of a copper paddlewheel. For both MOFs, the H_2 molecule position that was obtained from GCMC simulation was used as the initial position for the DFT calculations. All atoms of the MOF–H_2 system were permitted to vary, but the lattice parameters were kept constant. These calculations were implemented with the CP2K simulation package[10] using MOLOPT basis sets at the triple ζ level of theory,[11,12] Perdew–Burke–Ernzerhof (PBE) pseudopotentials,[13,14] and dispersion treated by the revised Vydrov–Van Voorhis nonlocal van der Waals density functional.[15] A section of the crystal structure of Cu-ATC and Cu-BTC showing the optimized H_2 molecule position about the copper paddlewheels are displayed in Figures S10(a) and S10(b), respectively. The adsorption energy (ΔE) for the H_2 molecule localized at the energy minimum position in both MOFs was calculated by the following:

$$\Delta E = E\,(\mathrm{MOF} + \mathrm{H_2}) - E\,(\mathrm{MOF}) - E\,(\mathrm{H_2}) \tag{3}$$

where $E(\mathrm{MOF} + \mathrm{H_2})$ is the energy of the unit cell of the MOF with the H_2, $E(\mathrm{MOF})$ is the energy of the empty unit cell, and $E(\mathrm{H_2})$ is the energy of the H_2. The calculated ΔE value for the optimized position of H_2 localized between Cu^{2+} ions of adjacent copper paddlewheels in Cu-ATC is -17.01 kJ mol^{-1}, which is close in magnitude to the experimental initial H_2 Q_{st} value for the MOF (12.63 kJ mol^{-1}). The ΔE value for the optimized position of H_2 about a single Cu^{2+} ion in Cu-BTC was calculated to be -12.23 kJ mol^{-1}. While the magnitude of this value is somewhat higher than the zero-loading H_2 Q_{st} value for the MOF (6.76 kJ mol^{-1}), it is still lower than the corresponding value that was calculated for Cu-ATC by *ca.* 5 kJ mol^{-1} (similar to the difference in the initial H_2 Q_{st} between the two MOFs), thus demonstrating that the Cu^{2+}–H_2 interaction in Cu-BTC is weaker than that in Cu-ATC.

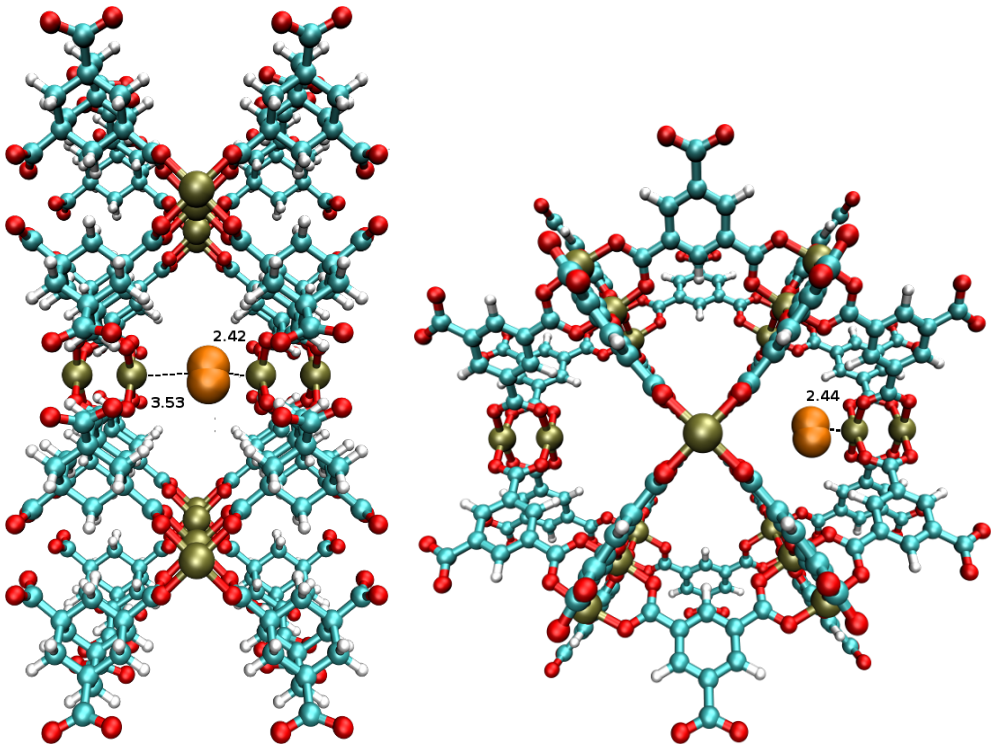

(a) Cu-ATC (b) Cu-BTC

Figure S10. Molecular illustration of the optimized position of a H_2 molecule (orange) localized **(a)** between the Cu^{2+} ions of adjacent copper paddlewheels in Cu-ATC and **(b)** about a single Cu^{2+} ion in Cu-BTC as determined from periodic DFT calculations using CP2K. Atom colors: C = cyan, H = white, O = red, Cu = tan.

Quantum Rotation Calculations

The two-dimensional quantum rotational levels for a H_2 molecule localized at the considered sites in Cu-ATC and Cu-BTC were calculated by diagonalizing the rigid rotor Hamiltonian in the spherical harmonic basis, Y_{jm}, which is given by eq S4:

$$\hat{H} = B\mathbf{j}^2 + V(\theta, \phi) \tag{4}$$

where B is the rotational constant for molecular H_2 (7.35 meV),[16] $\mathbf{j}^2$ is the angular momentum operator, and $V(\theta,\phi)$ is the potential energy surface for the rotation of the H_2 molecule with its center-of-mass held fixed within the MOF–H_2 system. In general, two-dimensional quantum rotation calculations involve solving equation S4 for a H_2 molecule within the field of the MOF by varying the θ and ϕ angles of the sorbate, but with the center-of-mass and H–H bond distance kept fixed. Each matrix element, $\langle Y_{jm}|V(\theta,\phi)|Y_{jm}\rangle$, was constructed using Gauss-Legendre quadrature[17] with a basis set consisting of $\pm m$ functions.[18] The rotational potential was generated over a 16 $\times$ 16 quadrature grid. The kinetic energy term, $j(j + 1)$, was added to the diagonal elements and the matrix was diagonalized using the LAPACK linear algebra package,[19] yielding the rotational eigenvalues and eigenvector coefficients. All two-dimensional rotational levels were calculated with $j = 7$, leading to 64 basis functions. All calculations were performed using the Massively Parallel Monte Carlo (MPMC) code, an in-house code that was developed and maintained in the Space research group.[20,21]

Hydrogen Potentials

Table S4. Parameters used to characterize the H_2 potentials used in this work: Buch model,[22] Belof Stern Space (BSS) model,[23] and polarizable Belof Stern Space Polar (BSSP) model.[23] COM corresponds to the center-of-mass site and OS corresponds to the off-atomic sites.

Model	Atomic Site	r (Å)	ϵ (K)	σ (Å)	q (e^-)	α° (Å^3)
Buch	COM	0.00000	34.20000	2.96000	0.00000	0.00000
BSS	COM	0.00000	8.85160	3.22930	-0.74640	0.00000
	H	0.37100	0.00000	0.00000	0.37320	0.00000
	OS	0.32900	4.06590	2.34060	0.00000	0.00000
BSSP	COM	0.00000	12.76532	3.15528	-0.74640	0.69380
	H	0.37100	0.00000	0.00000	0.37320	0.00044
	OS	0.36300	2.16726	2.37031	0.00000	0.00000

Additional Adsorption Results

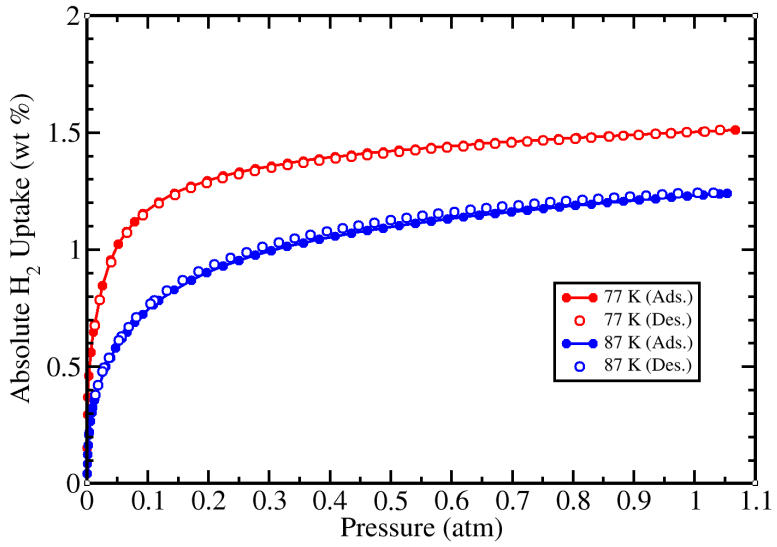

Figure S11. Experimental H_2 adsorption (closed circles with lines) and desorption (open circles) isotherms for Cu-ATC at 77 K (red) and 87 K (blue).

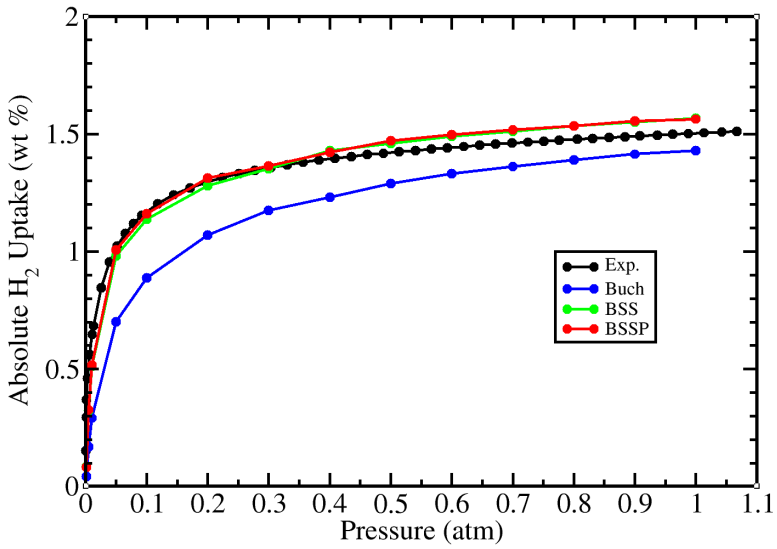

(a) 77 K

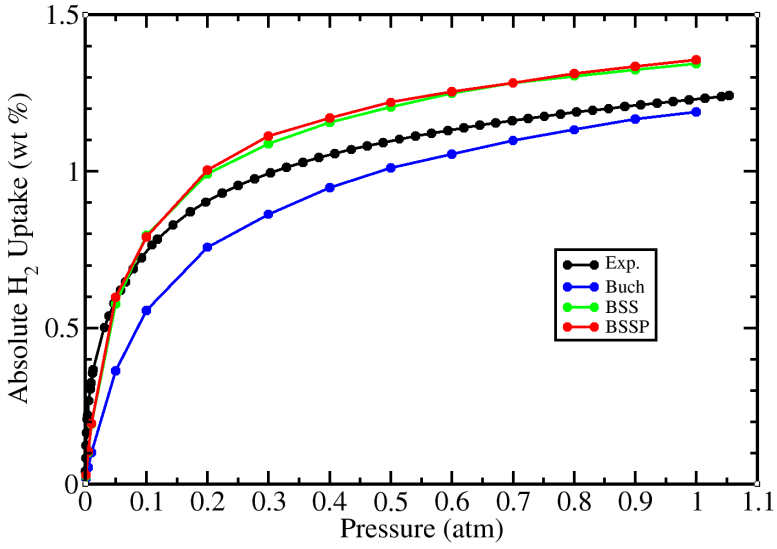

(b) 87 K

Figure S12. Absolute H_2 adsorption isotherms in Cu-ATC at **(a)** 77 K and **(b)** 87 K and pressures up to 1 atm for experiment (black) and simulations using three different H_2 potentials (Buch = blue, BSS = green, and BSSP = red).

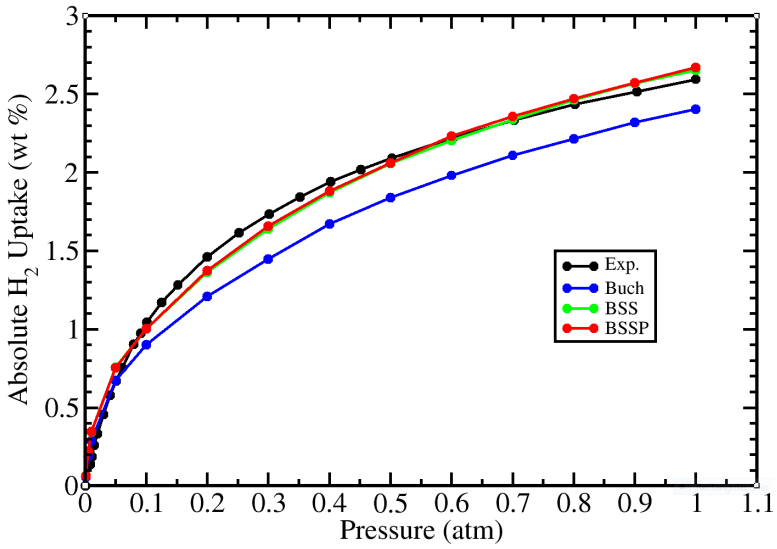

(a) 77 K

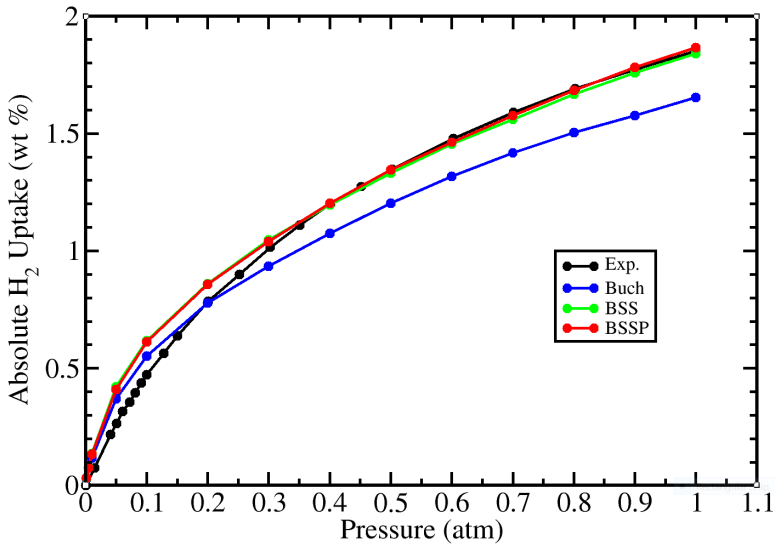

(b) 87 K

Figure S13. Absolute H_2 adsorption isotherms in Cu-BTC at **(a)** 77 K and **(b)** 87 K and pressures up to 1 atm for experiment (black) and simulations using three different H_2 potentials (Buch = blue, BSS = green, and BSSP = red). The experimental data were estimated from reference 24.

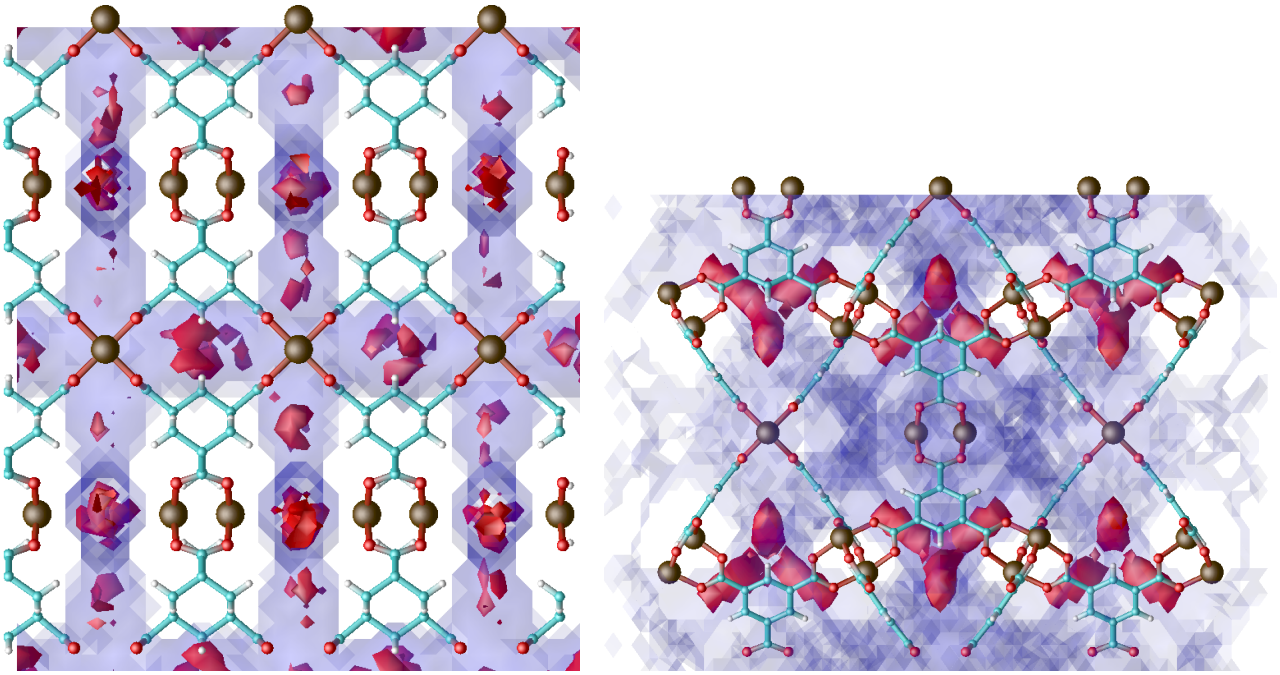

(a) Cu-ATC (b) Cu-BTC

Figure S14. Three–dimensional histogram of **(a)** Cu-ATC (orthographic a/b-axis view of 3 × 3 × 2 supercell) and **(b)** Cu-BTC (orthographic view of the 45° angle between two axes within a unit cell) showing the relative sites of H_2 occupancy (red = most frequently populated, violet = all populated) according to GCMC simulations using a polarizable H_2 potential at 77 K and 0.01 atm. Atom colors: C = cyan, H = white, O = red, Cu = tan.

[1] G. R. Newkome, A. Nayak, R. K. Behera, C. N. Moorefield and G. R. Baker, *J. Org. Chem.*, 1992, **57**, 358–362.
[2] Q. Fang, S. Gu, J. Zheng, Z. Zhuang, S. Qiu and Y. Yan, *Angew. Chem. Int. Ed.*, 2014, **53**, 2878–2882.
[3] B. Chen, M. Eddaoudi, T. M. Reineke, J. W. Kampf, M. O'Keeffe and O. M. Yaghi, *J. Am. Chem. Soc.*, 2000, **122**, 11559–11560.
[4] Z. Niu, X. Cui, T. Pham, P. C. Lan, H. Xing, K. A. Forrest, L. Wojtas, B. Space and S. Ma, *Angew. Chem. Int. Ed.*, 2019, **58**, 10138–10141.
[5] Z. Niu, X. Cui, T. Pham, G. Verma, P. C. Lan, C. Shan, H. Xing, K. A. Forrest, S. Suepaul, B. Space, A. Nafady, A. M. Al-Enizi and S. Ma, *Angew. Chem. Int. Ed.*, 2021, **60**, 5283–5288.
[6] Z. Niu, Z. Fan, T. Pham, G. Verma, K. A. Forrest, B. Space, P. K. Thallapally, A. M. Al-Enizi and S. Ma, *Angew. Chem. Int. Ed.*, 2022, **61**, e202117807.
[7] L. Czepirski and J. JagieŁŁo, *Chem. Eng. Sci.*, 1989, **44**, 797–801.
[8] M. Dincă, A. Dailly, Y. Liu, C. M. Brown, D. A. Neumann and J. R. Long, *J. Am. Chem. Soc.*, 2006, **128**, 16876–16883.
[9] R Development Core Team, *R: A Language and Environment for Statistical Computing*, R Foundation for Statistical Computing, Vienna, Austria, 2008.
[10] T. D. Kühne, M. Iannuzzi, M. Del Ben, V. V. Rybkin, P. Seewald, F. Stein, T. Laino, R. Z. Khaliullin, O. Schütt, F. Schiffmann, D. Golze, J. Wilhelm, S. Chulkov, M. H. Bani-Hashemian, V. Weber, U. Borštnik, M. Taillefumier, A. S. Jakobovits, A. Lazzaro, H. Pabst, T. Müller, R. Schade, M. Guidon, S. Andermatt, N. Holmberg, G. K. Schenter, A. Hehn, A. Bussy, F. Belleflamme, G. Tabacchi, A. Glöß, M. Lass, I. Bethune, C. J. Mundy, C. Plessl, M. Watkins, J. VandeVondele, M. Krack and J. Hutter, *J. Chem. Phys.*, 2020, **152**, 194103.
[11] J. VandeVondele and J. Hutter, *J. Chem. Phys.*, 2003, **118**, 4365–4369.
[12] J. VandeVondele and J. Hutter, *J. Chem. Phys.*, 2007, **127**, 114105.
[13] J. P. Perdew, K. Burke and M. Ernzerhof, *Phys. Rev. Lett.*, 1996, **77**, 3865–3868.
[14] J. P. Perdew, K. Burke and M. Ernzerhof, *Phys. Rev. Lett.*, 1997, **78**, 1396–1396.
[15] O. A. Vydrov and T. Van Voorhis, *J. Chem. Phys.*, 2010, **133**, 244103.
[16] J. Bigeleisen and M. G. Mayer, *J. Chem. Phys.*, 1947, **15**, 261–267.
[17] M. Abramowitz, *Handbook of Mathematical Functions with Formulas, Graphs, and Mathematical Tables*, Dover Publications, Inc., Mineola, NY, 1965.
[18] J. L. Belof, *Ph.D. thesis*, University of South Florida, 2009.
[19] E. Anderson, Z. Bai, J. Dongarra, A. Greenbaum, A. McKenney, J. Du Croz, S. Hammerling, J. Demmel, C. Bischof and D. Sorensen, Proceedings of the 1990 ACM/IEEE conference on Supercomputing, 1990, pp. 2–11.
[20] J. L. Belof and B. Space, *Massively Parallel Monte Carlo (MPMC)*, Available on GitHub, 2012, `https://github.com/mpmccode/mpmc`.
[21] D. M. Franz, J. L. Belof, K. McLaughlin, C. R. Cioce, B. Tudor, A. Hogan, L. Laratelli, M. Mulcair, M. Mostrom, A. Navas, A. C. Stern, K. A. Forrest, T. Pham and B. Space, *Adv. Theory Simul.*, 2019, **2**, 1900113.
[22] V. Buch, *J. Chem. Phys.*, 1994, **100**, 7610–7629.
[23] J. L. Belof, A. C. Stern and B. Space, *J. Chem. Theory Comput.*, 2008, **4**, 1332–1337.
[24] J. L. C. Rowsell and O. M. Yaghi, *J. Am. Chem. Soc.*, 2006, **128**, 1304–1315.